Vapor-Phase Infiltration inside a Microporous Porphyrinic Metal–Organic Framework for Postsynthesis Modification

Siddhartha De, Gia Co Quan, Ben Gikonyo, Charlotte Martineau-Corcos, Colin Bousige, Laurent Veyre, Thomas Devic, Catherine Marichy, Alexandra Fateeva

Vapor Phase Infiltration inside a Microporous Porphyrinic Metal Organic Framework for Post Synthesis Modification

Siddhartha De,[a] Gia Co Quan,[a] Ben Gikonyo,[a] Charlotte Martineau Corcos,[b,c,d] Colin Bousige,[a] Laurent Veyre,[e] Thomas Devic,[f] Catherine Marichy[a] and Alexandra Fateeva*[a]

a Univ Lyon, Université Claude Bernard Lyon 1, Laboratoire des Multimatériaux et Interfaces (LMI), UMR CNRS 5615, F-69622 Villeurbanne, France.
b ILV UMR CNRS 8180, Université de Versailles St-Quentin en Yvelines, Université Paris Saclay, 78035 Versailles, France.
c CEMHTI UPR CNRS 3079, Université d'Orléans, F-45071 Orléans, France.
d Institut Universitaire de France (IUF), 75231 Paris Cedex 05, France.
e Univ de Lyon, Laboratoire de Chimie, Catalyse, Polymères et Procédés, UMR CNRS 5265, F- 69616Villeurbanne, France.
f Institut des Matériaux Jean Rouxel (IMN), UMR 6502, Université de Nantes, CNRS, 2 rue de la Houssinière, BP32229, 44322 Nantes cedex 3, France.

ABSTRACT: Vapor Phase Infiltration (VPI), a technique derived from Atomic Layer Deposition (ALD) and based on sequential self-limiting chemistry is used to modify the stable microporous porphyrin-based Metal Organic Framework (MOF) MIL-173(Zr). VPI is an appealing approach to modify MOFs by inserting reactants with atomic precision. The microporous nature and chemical stability of MIL-173 enable post-synthesis modification by VPI without MOF degradation even with extremely reactive precursors such as trimethylaluminum (TMA) and diethylzinc (DEZ). VPI proceeds through the diffusion of gaseous organometallic reactants TMA and DEZ inside the microporous framework where they react with two kinds of chemical sites offered by the porphyrinic linker (phenolic functions and pyrrolic functions in the porphyrin core), without altering the crystallinity and permanent porosity of the MOF. ^{27}Al NMR, UV-vis absorption and IR spectroscopies are used to further characterize the modified material. Physisorption of both precursors is computationally simulated by Grand Canonical Monte Carlo methods and outlines the preferential adsorption sites. Impact of temperature, number of VPI cycles and pulse length are investigated and show that, Al and Zn are introduced in a saturating manner inside the MOF on both available reactive sites. Porosity prerequisite is outlined for VPI which is proven to be much more effective than classical solution-based methods as it is solventless, fast, prevents work-up steps and allows reactions not possible by classical solution approach.

INTRODUCTION

Due to the key role of tetrapyrrolic complexes in natural systems, their synthesis and coordination chemistry have been fascinating scientists for more than a century. More recently supramolecular chemistry demonstrated that these compounds could be assembled in a controlled manner to study and rationalize associated molecular and photophysical interactions. In this area, Metal Organic Framework (MOF) elaboration can be seen as an accessible way to organize porphyrins and phthalocyanines in space in an ordered manner. The versatility of MOF chemistry allowed access of multiple compounds where parameters such as the inorganic building unit, the metalloporphyrin and the porosity could be tuned[1,2]. On top of this, MOFs could be altered through post-synthesis modification (PSM), a strategy that grants new functionality while preserving the structure of the network[3–5]. In this field, some porphyrin-based MOFs can be visualized as pertinent examples. Indeed, when the structural framework metal does not coordinate the tetrapyrrolic motif, which is the case for high valency metals such as aluminum and zirconium, post-synthesis porphyrin metalation has proven effective to impart new functionality such as oxidation catalysis[6,7], oxygen reduction reaction electrocatalysis[8], CO_2 photoreduction[9,10] and so on. In all these studies, PSM was performed by solution chemistry, involving time-consuming steps for the reaction, solid isolation and reactivation. An alternative PSM strategy is to use vapor phase approaches, among which atomic layer deposition (ALD) was recently demonstrated to be compatible with MOF chemistry[11,12](with some limitations, see below). ALD is a unique technique based on self-limiting successive reactions usually applied for deposition of conformal and homogeneous thin films[13]. More recently an increasing number of studies have reported ALD inside polymeric and porous structures[14–17]. Since the reactions occur at the vapor/solid interface, this approach is solventless and thus avoids both competitive adsorption of solvent (*vs.* reactant) and time-consuming work up steps.

Vapor phase infiltration (VPI) can be seen as an ALD derived process where a single precursor can be used to react at the vapor/solid interface[15]. More precisely, during VPI an in-depth diffusion of precursors is observed inside a solid.

Regarding tetrapyrrolic compounds, vapor phase metalation has recently attracted attention to better understand the interfacial chemistry of the macrocycles[18]. If most studies addressed 2-D on-surface architectures, 3-D and multilayer systems metalations still remain challenging. The proof of concept of porphyrin nanoaggregates metalation using ALD was established by Zhang *et al.* who used diethylzinc (DEZ) and H_2O for encapsulation of these nanostructures by ZnO[19]. The authors observed partial metalation of porphyrins while the supramolecular structure was preserved, indicating that DEZ could diffuse into the interior of porphyrinic supramolecular filaments. Such an infiltration of metal precursors and further metalation was not observed upon exposure to trimethylaluminum (TMA) and titanium isopropoxide during Al_2O_3 or TiO_2 coatings, suggesting that the size of the precursor molecules played a critical role. Vapor-phase growth of metalloporphyrin multilayer was demonstrated by Kim *et al.* using a sequential approach[20]. By alternatively evaporating free-base porphyrin on a surface and then exposing it to DEZ vapor that reacted with pyrrolic nitrogen in self-limiting manner, 100 nm thick hybrid thin film was achieved. Site-selective ALD took advantage of porphyrins covalently linked to a surface as nucleation sites to allow metalloclusters growth as spatially separated islands[21]. $Mn(CpEt)_2$ precursor was used in vapor phase, to produce Mn-porphyrin that presented an anchoring site through Mn axial coordination for MnO growth. However, the same strategy was not successful with more reactive DEZ or TMA precursors and degradation of porphyrins was observed. This short survey instructs that VPI and ALD have led to metal insertion in porphyrins with a diffusion path of few nanometers (single layer or nano-agregates) and were efficient only in case of divalent metals.

In the field of MOFs, ALD was first employed to grow metal oxide layer on substrates in order to facilitate MOF growth[22–25]. Later it was implemented for PSM, in all the studies a metallic precursor and water were used successively to grow metal oxide/hydroxide clusters inside the porous framework or on top of the MOF crystallites. Due to the challenge of the ALD process in high aspect ratio and nanoporous materials[17,17,26–28], research has been mostly focused on the mesoporous MOF NU-1000. Indeed, the first example was reported in 2013,[29] and since then almost all studies have focused on Zr_6-based frameworks, among which only NU-1000 and UiO-66 were studied in depth[11,12,30–36]. Both are formed by $Zr_6O_4(OH)_4$ nodes with reactive OH groups therefore ALD reactions occur at the inorganic unit. Even if the implication of the amino group from the linker was demonstrated in case of UiO-66 (NH_2),[12] ligand-centered ALD process was not focused by these studies. Only very recently, Yang *et al.* reported VPI of the porphyrin-based Al-PMOF[37], by using DEZ and H_2O; they showed ZnO clusters growth in the porous structure along with Zn insertion inside the porphyrin core[38].

On the other hand, aiming to insert isolated metallic sites rather than clusters, VPI can be used through pulse and purge cycles of a single organometallic precursor and has recently generated interest for modification of organic polymers[15,39]. Regarding MOF PSM this approach would allow precisely reacting metal precursors only at available sites and thus reach reactions that are intricate through classical PSM. Yet single precursor VPI has not been studied in the field of microporous MOFs.

Our study focuses on the microporous MIL-173 (Zr) framework, where the inorganic unit is a chain of edge-sharing ZrO_8 dodecahedra originating from the oxygen coordination of a trihydroxyphenyl-porphyrin (porphGal). The chemical formula of the activated MOF is $Zr_2(H_6porphGal)$ [6]. The reactive sites for VPI originate from the porphyrinic ligand and therefore a different reactivity compared to the previous studies is observed. The exceptional chemical stability of MIL-173(Zr) allows VPI with highly reactive precursors such as DEZ and TMA, even though the latter was earlier shown to degrade hydrolytically stable Zr-carboxylate frameworks[11,34]. In our work we demonstrate that arranging porphyrins in a porous framework enables an easy and fast metalation with the advantages of the VPI process and thus provides an efficient way to high valent metal insertion that are difficult through conventional solution methods.

RESULTS AND DISCUSSION

Reactive sites available for VPI in MIL-173.

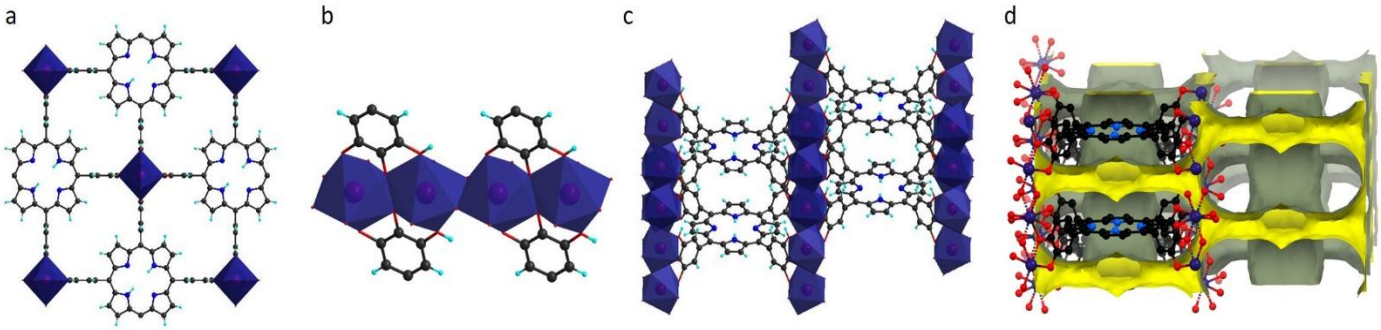

Figure 1: MIL-173 structure displaying: (a) pyrrolic sites (b) phenolic sites (c) porphyrinic arrangement along the c axis (d) porous volume accessible by 1.5 Å radius probe. Atomic color code: C (black), N(blue), O(red), H (cyan), Zr (violet).

As reported recently, MIL-173 is a robust 3D metal organic framework formed by Zr(IV) chains that lie perpendicular to porphyrinic ligands[6] (Figure 1). The coordination of Zr(IV) ions is fully completed by the oxygen atoms from the porphyrinic linker, which prevents the presence of additional hydroxo or oxo ligands like in NU-1000 and UiO-66. In the case of MIL-173, the reactive sites for VPI are provided by the linker. Indeed, one of the phenolic groups (meta position) remain protonated when the oxygen coordinates Zr(IV), leading to an acidic proton (Figure 1b) that can potentially be replaced by a metallic ion. Additionally, the porphyrin core is in the free base form, which provides a second site accessible for PSM metal insertion (Figure 1a). These two reactive sites would provide a potential maximum insertion of 5 metals per porphyrin, i.e. 2.5 metals per Zr. The same topology framework is obtained when Zr(IV) is replaced by La(III), displaying more phenolic protons for charge balance, showing the same free base porphyrin core but with less robustness.

In the MIL-173 framework pores run in 3 dimensions. Between the porphyrins, pores of 16 Å free diameter and 4 Å thickness are interconnected with perpendicular elliptic channels of ca. 9 ×4 Å free aperture size (Figure 1d and see reference 6 for more details). When MIL-173(Zr) is an intrinsically porous material with a type-I N_2-sorption isotherm and a BET surface area of ~ 850 $m^2.g^{-1}$, MIL-173(La) collapses upon classical activation procedure and only negligible accessible porosity can be measured by N_2 sorption.

To sum up, the adaptability of the secondary building unit of the trioxobenzene linker leads to very similar structures with Zr(IV) and La(III) displaying the same reactive sites but with very different stabilities and intrinsic porosities. This feature is convenient to demonstrate the stability and porosity impact on VPI in MOFs.

General experimental considerations.

Our study focusses mainly on the chemically stable MIL-173(Zr) framework. For comparison, VPI was also implemented on non-intrinsically porous compounds: the MIL-173(La) as well as on molecular species: the tetraphenyl and trihydroxy-phenyl porphyrins. TMA and DEZ were tested for the PSM of MIL-173 as they are among the most common ALD precursors. More importantly, they are different in size and shape and allow reactivity comparison between a trivalent and divalent metal on two different sites of the MOF (note that in an earlier study, only DEZ was infiltrated in a porphyrin contrary to TMA[19]). Solid state ^{27}Al NMR spectroscopy allowed deeper structural investigations in the case of TMA deposition. Our goal was to achieve PSM on isolated specific sites of the MOF rather than growing a metal oxide/hydroxide layer. For this reason, a process of organometallic precursors pulses followed by purge was implemented, without the use of water as co-reactant, which can be seen as a half-cycle ALD process. Microcrystalline MOF samples were each time heated under vacuum inside the ALD reactor to remove any adsorbed water molecules to prevent un-controlled nucleation sites. Typically,

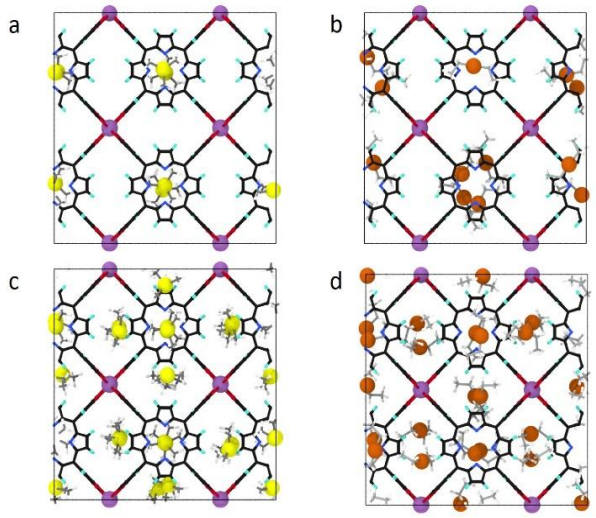

Figure 2: (a-c) TMA and (b-d) DEZ adsorbed in a unit cell of MIL-173 as obtained from GCMC simulations at (a-b) 2.10^{-3} Pa and (c-d) 10^4 Pa. The atomic color code is the same as in Figure1, with the adsorbed molecules represented with C (gray), H (white), Al (yellow) and Zn (brick).

successive precursor pulse/purge cycles (0.3 s and 15 s respectively) were used to infiltrate the organometallic precursor, keeping in mind that when the product was recovered in air, spontaneous hydrolysis of reactive organometallic bonds would occur. To understand the effect of the exposure time, experiments with one long precursor pulse (120 s) followed by 15 minutes purging were performed.

Precursors diffusion inside the pores.

When pore sizes are close to the size of the precursor molecule, the diffusion may be challenging. To check whether MIL-173(Zr) was able to accommodate TMA and DEZ molecules, Grand Canonical Monte Carlo (GCMC) adsorption simulations were carried out at a temperature of 50 °C (same as the experimental one) and pressures varying between 10^{-6} Pa and 10^4 Pa. The results showed that both TMA and DEZ could be adsorbed by MIL-173(Zr) (Figure 2). At low pressure, the first preferred adsorption sites are lying in-between the porphyrinic macrocycles, which stabilizes the adsorbate by maximizing weak intermolecular interactions (Figure 2 a and b). This result is in line with what was reported before in the case of NU-1000 where the preferential adsorption sites were located into the most confined small triangular pores. At the highest pressure, the GCMC-obtained metal:Zr ratio is of 1.6 in both cases (Figure 2 c and d and Figure S1) – that is, without considering the reactivity of the adsorbed molecules with the framework.

Interestingly, the GCMC simulations showed that the *dimeric* form of TMA could not be adsorbed and diffuse in MIL-173, only the *monomeric* form could do so. As the dimer/monomer thermodynamic equilibrium in vapor phase depends on the temperature[40], its effect on the outcome of VPI was considered.

Vapor phase infiltration of TMA.

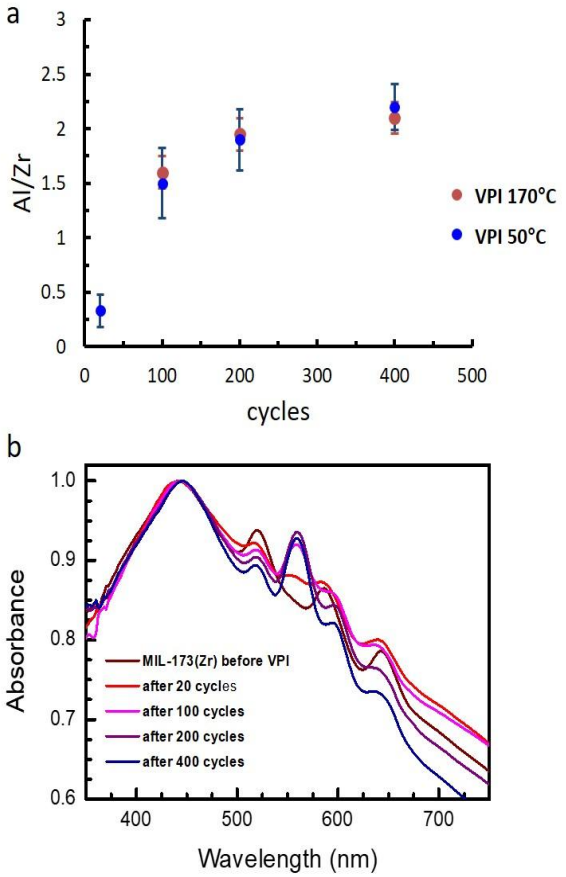

Figure 3: (a) Al/Zr ratio along the VPI cycles at 50 °C and 170 °C from SEM/EDS analysis, (b) Solid state UV-vis spectra of Al-MIL-173(Zr) along VPI cycles at 50 °C.

As stated above, TMA is well-known to be at equilibrium between dimeric (low temperature, 50 °C in this work) and monomeric (high temperature, 170 °C in this work) forms. Temperature influence on TMA diffusion in MIL-173 was therefore examined. The amount of Al added to the MOF structure along TMA pulsing at 50 °C and 170 °C was monitored by energy dispersive spectroscopy (EDS) analysis using scanning electron microscopy (SEM). The Al/Zr ratio tends to a plateau at around 2.1 (+/-0.2) after 400 cycles in both cases (Figure 3a) which agrees with the total available 2.5/Zr sites in the MIL-173 structure. This indicates that both the phenolic and the pyrrolic functions are modified by Al insertion, leading to a new material, named Al-MIL-173(Zr). Unexpectedly, using low or high temperature does not influence the outcome of the VPI to a noticeable extent. This suggests that TMA is dissociated when it starts to interact with the MOF surface. Which is in line with the GCMC calculations: the TMA-MOF surface interaction energy reaches ca. 30 kcal.mol^{-1}, to be compared with the rather low binding energy of the dimeric TMA[41] (4.2 kcal.mol^{-1}).

Powder X-Ray Diffraction (PXRD) data (Figures 4a, S2, S3 and S4) demonstrate that the crystallinity of MIL-173(Zr) is preserved after VPI both at 50 °C and 170 °C. Absence of any crystallized metal or metal oxide/hydroxide is evidenced by PXRD (Figure S16). Moreover, the sample remains microporous with a

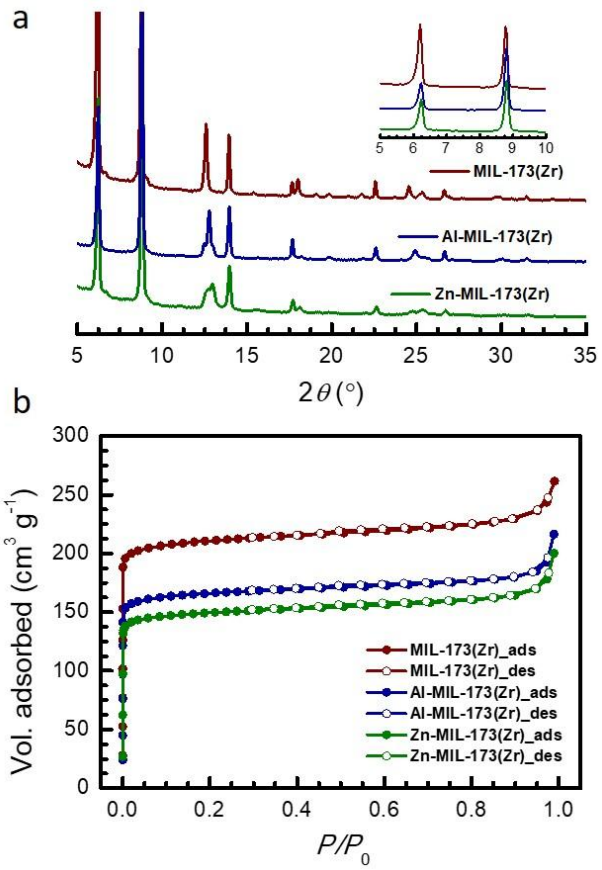

Figure 4: (a) PXRD data and (b) N_2 sorption isotherms measured at 77.3K for MIL-173(Zr) before and after 400 VPI cycles of TMA and DEZ at 50°C.

decrease of the BET surface area (BET SA) from 850 m^2.g^{-1} to 665 m^2.g^{-1} and 690 m^2.g^{-1} for VPI at 50 °C and 170 °C respectively, along with the decrease of the porous volume from 0.4 to 0.34 cm^3.g^{-1} (Figure 4b and S6). This indicates that Al gets incorporated inside the porous structure of MIL-173 and attests of the exceptional stability of this MOF whereas NU-1000 was reported to significantly degrade when reacted with TMA[34]. The morphology of MIL-173(Zr) crystallites remain unchanged by the VPI process using both high and low temperature as evidenced from SEM images (Figure S12).

VPI using a single long pulse.

VPI of MIL-173(Zr) proceeds extremely quickly and efficiently, compared to classical solution based reactions and to VPI of porphyrinic monolayers where pulses of several seconds were applied[20]. To check the effect of a longer TMA exposure time, the process was performed only with a single precursor pulse of 120 seconds, followed by a 15 minutes purge (note that 120 s is equivalent in time to 400 cycles of 0.3 s pules). Here again the reaction temperature did not have a meaningful effect as at 50 °C and 170 °C the Al/Zr ratio in the resulting material were of 0.85 and 0.8 respectively. The samples keep their

morphology, crystallinity and microporous nature as evidenced from SEM, PXRD and nitrogen sorption isotherms (Figures S9, S10 and S12). The BET SA value decreases from 850 $m^2.g^{-1}$ to 730 $m^2.g^{-1}$, confirming Al insertion inside the pores but to a lesser extent compared to what is observed with multiple short pulse process. This observation appears coherent in the sense that removing co-products (CH_4) and unreacted TMA during the purge cycles liberates pore space for better precursor diffusion in the following cycles, leading to a more efficient reaction with more available sites in the MOF. It can be outlined that a 120 s pulse incorporates roughly the amount of Al that can be inserted after approx. 60 short pulse cycles. Therefore, a single pulse (that could be performed easily in any laboratory without the need of automatic ALD equipment) leads to an efficient reaction of TMA with MIL-173, but successive pulse/purge cycles provide a way to reach higher Al infiltration.

The VPI process thus appears as extremely effective for MOF PSM even with relatively low temperature and short precursor pulsing time. As a standard PSM procedure, 400 pulse/purge cycles were applied at 50 °C for TMA infiltration of up to 100 mg MOF powder sample. Al/Zr ratios were measured each time and varied from 1.9 to 2.1 in different batches.

Spectroscopic characterizations of Al-MIL-173(Zr)

To assess the Al insertion inside the porphyrin core, UV-vis spectroscopy was used to monitor the modification of absorption spectra as a function of the number of TMA pulsing cycles. In fact, porphyrinic compounds display characteristic UV-vis absorption features dominated by π-π transitions, which get strongly affected by a metal insertion in the center of the macrocycle. As shown on Figure 3b solid-state UV-vis absorption of the starting material presents a strong Soret absorption band at 446 nm and three Q bands at 520, 585 and 645 nm. When exposed to TMA, the UV-vis absorption features change gradually along the number of cycles. In particular, a new absorption band in the visible region rises at 560 nm, while the intensity of the original three Q bands decreases and the band at 585 nm is red-shifted to 600 nm. The Q bands in the resulting spectrum are dominated by two strongest absorptions (560 and 600 nm), which are characteristic of metalated porphyrins[42]. Metalation of the porphyrinic core through a single long pulse also occurs to a noticeable extent, as shown by the change of the UV-vis absorption spectra (Figure S11). This attests that rather than only reacting on the surface of crystallites, TMA efficiently diffuses inside the microporous structure and reacts with the pyrrolic sites even with short pulses and without any exposure time.

As two types of reactive sites are available in the MOF network (phenolic OH and pyrrolic NH) one would question whether one of the sites is more reactive than another. In a recent study, TMA reactivity with different organic functions was compared; the lowest activation energy was evidenced for a phenolic OH group compared to an aromatic NH_2 function[43]. Nonetheless, TMA reactivity with porphyrinic pyrroles was not described until now. In our case, the very gradual change of the UV-vis spectra and the Al/Zr ratio increase along with TMA short pulse cycles suggest that both OH and pyrrolic sites react with TMA simultaneously.

To further understand Al infiltration, solid-state ^{27}Al NMR spectroscopy was performed. The ^{27}Al magic-angle spinning (MAS) NMR spectrum of Al-MIL-173(Zr) (Figure 5a) shows the presence of four resonances corresponding to Al atoms on four chemically distinct sites. The weak signal at around 70 ppm is characteristic of Al in tetrahedral oxygenated environment, the signal centered on 30 ppm is characteristic of penta-coordinated Al, the one at 5 ppm corresponds to an Al in octahedral geometry[44] while the signal at negative chemical shift (-20 ppm) originates from an hexacoordinated Al inside the porphyrinic macrocycle[45] with very likely OH and H_2O axial ligands completing the coordination sphere and charge balance. The NMR spectrum therefore indicates that, on top of metalating the porphyrin, TMA reacts with other available sites in the MIL-173 structure, generating Al centers corresponding to NMR signals very close to the ones found in aluminum oxide and hydroxide. As described earlier, the other available reactive site is the phenolic oxygen where the acidic proton can be partially replaced by Al. After exposure to air, this would give rise to Al sites in fully oxygenated coordination environments originating from the phenolic oxygen(s), and OH/H_2O ligands. The ^{27}Al resonances are broad and featureless, indicating local structural disorder around the Al atoms, in agreement with the various possible environments (OH or H_2O ligands). Further information about the Al geometry was obtained by ^{27}Al NMR multiple-quantum MAS (MQMAS) NMR (Figure 5b). Such experiment provides separation of the contribution from the chemical shift distribution, which spreads the signal along the diagonal, and the quadrupolar

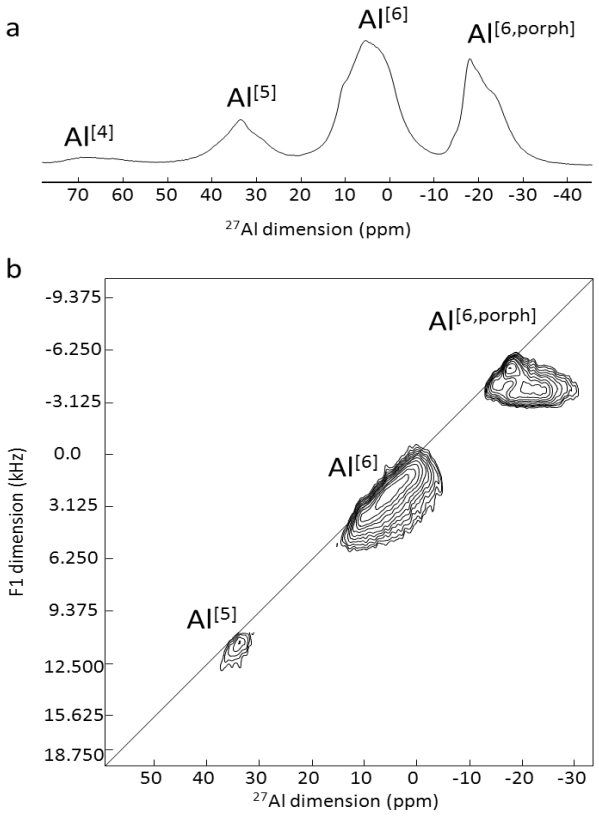

Figure 5. ^{27}Al MAS (a) and MQMAS (b) NMR spectra of Al-MIL-173(Zr) obtained after VPI at 50°C, 400 cycles. The lines are assigned.

interaction (originating from the nuclear spin of the ^{27}Al nucleus which is greater than ½), which shifts the resonances along the horizontal dimension (the larger the interaction, the more shifted to the right the resonance). On the ^{27}Al MQMAS NMR spectrum of Al-MIL-173(Zr) (Figure 5b), one can notice very different line shapes between the two types of hexacoordinated aluminum atoms (Al[6] and Al[6, porph]). The signals of Al surrounded by oxygen atoms Al[6] (around 5 ppm) and Al[5] (Al[4] signal is too weak and could not be detected) show significant chemical shift distribution, which attests of a distribution of chemical/geometrical environments around the Al sites. Contrastingly, the signal at -20 ppm is composed of two small lines along the diagonal and a resonance of much higher intensity with a large quadrupolar coupling constant (C_Q) of 8.2 MHz (Figure S14). This later corresponds to the Al atoms lying in the porphyrin core and which have a very constrained environment. Deconvolution indicates that about 30% (+/- 6%) of the Al is incorporated in the porphyrin core (Figure S10). This ensemble of ^{27}Al NMR data confirms that Al can be incorporated in all the available reactive sites in MIL-173: Al can be inserted in the porphyrin, where it gets coordinated by 4 nitrogen atoms from the MOF, leading to a confined and well-defined environment, or it can be coordinated by 1 or 2 phenolic oxygen atoms, with a distribution of geometries with OH and water to complete the coordination sphere of Al. Deconvolution result of NMR data indicates that Al insertion inside the porphyrin core is quasi-quantitative.

Diffuse Reflectance Infrared Fourier Transform Spectroscopy (DRIFTS) analysis was used to further understand the PSM of MIL-173. Due to the high acidity of the phenolic OH in the parent MOF, its stretching vibration is shifted to lower energy and is overlapped with the pyrrolic NH stretching vibration signal[46] between 3300 and 3360 cm^{-1}. After exposure to TMA, the intensity of the broad peak weakens noticeably and a broad band originating from H_2O and OH that complete the Al coordination sphere appears at 3550-3350 cm^{-1} (Figure S15). The overlap of the signals makes it delicate to unambiguously interpret the data in this region, however two additional bands appear on the DRIFT spectrum after TMA VPI at 1010 and 950 cm^{-1}. These wavenumbers correspond well to OH bending vibrations described for Al-OH functions in gibbsite[47], in line with the results of the NMR analysis.

Vapor phase Infiltration of DEZ.

A similar study was undertaken with DEZ precursor. Both multiple pulse/purge cycles and a single long pulse were applied for MIL-173(Zr) PSM at low (50 °C) and high (170 °C) temperatures. The obtained Zn-MIL-173(Zr) MOF solids remained crystalline and porous in all cases (Figures 4, S2 and S5), confirming the robustness of the framework and the adaptability of the process to another precursor in a wide range of operating temperatures. Again, absence of any metal or metal oxide/hydroxide was verified by PXRD (Figure S21).

When short pulse VPI was performed, porphyrin metalation could be monitored along the pulses (Figure S7). During Zn insertion, main changes appear in the visible region: the relative intensities of the absorption bands at 520 nm and 640 nm decrease, a new band rises at 558 nm and the band at 585 nm is shifted to 595 nm. The saturation of VPI is reached after 400 cycles at 50°C for a Zn/Zr ratio of 1.8 as evidenced from SEM/EDS analysis. Like with TMA, the porosity of the final materials is preserved with a measured BET surface area of 598 $m^2.g^{-1}$ and a total pore volume of 0.31 $cm^3.g^{-1}$ (Figure 4b). Nevertheless, the final materials appeared less homogeneous than in the case of TMA in terms of Zn/Zr ratio observed in distinct crystallites. It might be due to a more demanding DEZ diffusion and/or ethane removal during the pulse and purge cycles respectively. Temperature did not show influence on the Zn insertion efficiency. Supposedly, VPI could be further optimized in the case of DEZ using longer cycles and/or exposure time that are efficient for more demanding diffusion.

Similarly to the case of TMA, the use of a long single pulse was found to be less efficient than short multiple pules. A single pulse of 120 s leads to a Zn/Zr average ratio of 0.6 and the porphyrin core metalation is slightly less effective as evidenced by solid state UV-vis spectroscopy. A limited decrease in the BET surface area from 850 to 730 $m^2.g^{-1}$ (Figure S10) is also measured.

Effect of porosity.

VPI inside microporous materials is known to be challenging. Therefore, to check the extent to which porosity influences the metal insertion, similar VPI experiments were performed on MIL-173(La) and simple molecular porphyrin solids (tetraphenyl porphyrin (TPP) and porphGal). As stated above, MIL-173(La) is an isostructural compound to MIL-173(Zr) (PXRD data in Figure S16) but it collapses upon activation, giving a BET SA of only of 10 $m^2.g^{-1}$ (Figure S17). TPP porphyrin offers only one potential metal insertion site in the porphyrin core when in porphGal phenolic functions are also available (Figure S19 a).

When exposed to TMA pulses, MIL-173(La) shows no Al incorporation from SEM/EDS analysis, neither changes in its UV-vis absorption features (Figure S18), demonstrating that intrinsic porosity is a prerequisite for successful VPI process. Molecular porphyrin solids were analyzed by UV-vis spectroscopy in solution (Fig S19) and SEM/EDS. Again, no metal infiltration could be detected and the UV-vis absorption features of both molecular species remain unchanged, confirming that the porphyrin core metalation does not occur in molecular compounds without porous structure. Hence the accessible porous structure of MIL-173 is crucial for effective VPI, as no PSM proceeds in analogous material without intrinsic porosity. This demonstrates that the VPI does not occur just though defects of the crystalline structure neither through a migration of reacted species from the outer surface of a crystallite towards the core.

Comparison with PSM in solution

Chemical reactions at low pressure and in vapor phase may not always follow the same course as in solvent,

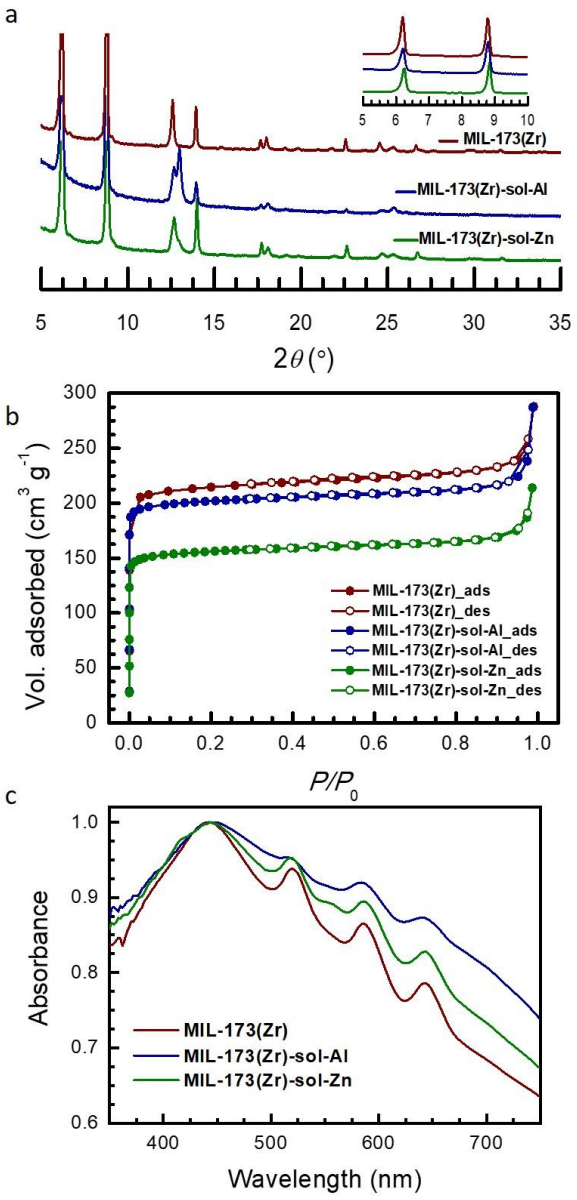

Figure 6: (a) PXRD data, (b) N_2 sorption isotherms measured at 77.3K and (c) UV-vis absorption spectra of MIL-173(Zr) before and after PSM in solution.

which stimulates the interest of getting products that are not achievable by classical wet chemistry methods. To compare PSM of MIL-173 in our case, we performed analogous metal infiltration tests in solution, using classical metallic precursors for solvent based methods (zinc and aluminum chloride). By reacting MIL-173(Zr) with either precursors at 50 °C in DMF for 2 h the MOF remain crystalline (Figure 6a) and porous. The BET SA (Figure 6b) does not undergo a noticeable decrease in case of Al (850 versus 820 $m^2.g^{-1}$ before and after PSM respectively), confirming the very low rate of Al infiltration. In the case of Zn, a decrease of the BET SA to 630 $m^2.g^{-1}$ is observed. However, the UV-vis spectra do not show a remarkable change (Figure 6c), meaning that most porphyrinic cores remain non metalated. Indeed, in the case of Zn, a small band at 558 nm appears suggesting a start of metal insertion after 2 h, while for Al the spectrum corresponds to the free base porphyrin. From SEM/EDS analysis after 2 h reaction, Al/Zr and Zn/Zr ratios of 0.1 and 0.14 respectively are quantified. These values suggest that in solution, Zn gets mainly inserted inside the porphyrin core while Al only reacts with the available phenolic sites given its oxophilic nature. While MIL-173(Zr) is stable both in case of solution and vapor PSM, this demonstrates that the metal insertions proceed faster and more efficiently through VPI, the vapor process being extremely beneficial for metal coordination inside the porous framework. During VPI, metallic precursors do not need to compete with solvent molecules inside the pores to diffuse and react promptly. More importantly, Al insertion in the porphyrin core is observed during VPI but not via classical solution-based methods.

CONCLUSIONS

In summary, we report here the feasibility and the efficiency of the VPI approach for PSM of a microporous porphyrin-based MOF displaying two types of reactive sites, evidencing that VPI is not restricted to mesoporous frameworks. This process is extremely convenient compared to classical solution based PSM and prevents laborious steps of solid recovery and solvents waste. Moreover, precursors diffusion in the micropores of MIL-173(Zr) is efficient, as much faster VPI is achieved here when compared to what is reported for organic polymers where long exposure times are needed for reactants to diffuse inside the sub-surface. MIL-173(Zr) shows considerable stability, enabling VPI with both DEZ and TMA, despite that the later one is an extremely reactive precursor that has been shown to degrade other stable Zr-based MOFs. This better tolerance to highly reactive organometallic reactants might be due to the fact that PSM occurs here solely on the linker rather than on the inorganic node, as it was the case for the Zr_6-based materials reported to date. In fact, modification of the inorganic secondary building unit can lead to a stronger impact on the overall framework integrity. The versatility of the VPI process for MIL-173(Zr) is an appealing feature, as here we observe that both divalent and trivalent metals could be efficiently introduced in the MOF on both OH and NH sites, which modifies its photophysical properties. Therefore, we expect this approach to be extendable to a number of VPI precursors enabling to tune MOF properties.

ASSOCIATED CONTENT

Supporting Information including experimental details, GCMC simulation details and complementary analysis data is available free of charge via the Internet at http://pubs.acs.org.

AUTHOR INFORMATION

Corresponding Author

* alexandra.fateeva@univ-lyon1.fr

Author Contributions

All authors have given approval to the final version of the manuscript.

Funding Sources

This work was supported by the French Research Agency ANR JCJC grant STREAM and by the regional Auvergne Rhone Alpes SCUSI project. The authors thank the French Ministry of National Education, Research and Technology, for PhD grant, the University Lyon 1 and the CNRS for financial support.

ACKNOWLEDGMENT

The authors thank the CTμ (Centre Technologique des Microstructures of University of Lyon) for providing the scanning electron microscopy facility. Financial support from the IR-RMN-THC Fr3050 CNRS and the Ile-de-France DIM 'RESPORE' is acknowledged.

REFERENCES

1. Gao, W.-Y., Chrzanowski, M. & Ma, S. Metal–metalloporphyrin frameworks: a resurging class of functional materials. *Chem. Soc. Rev.* **43**, 5841–5866 (2014).
2. Feng, L., Wang, K.-Y., Joseph, E. & Zhou, H.-C. Catalytic Porphyrin Framework Compounds. *Trends Chem.* (2020) doi:10.1016/j.trechm.2020.01.003.
3. Tanabe, K. K. & Cohen, S. M. Postsynthetic modification of metal–organic frameworks—a progress report. *Chem. Soc. Rev.* **40**, 498–519 (2011).
4. Evans, J. D., Sumby, C. J. & Doonan, C. J. Post-synthetic metalation of metal–organic frameworks. *Chem. Soc. Rev.* **43**, 5933–5951 (2014).
5. Wang, Z. & Cohen, S. M. Postsynthetic modification of metal–organic frameworks. *Chem. Soc. Rev.* **38**, 1315–1329 (2009).
6. Mouchaham, G. *et al.* Adaptability of the metal(iii,iv) 1,2,3-trioxobenzene rod secondary building unit for the production of chemically stable and catalytically active MOFs. *Chem. Commun.* **53**, 7661–7664 (2017).
7. Wang, X.-S., Chrzanowski, M., Wojtas, L., Chen, Y.-S. & Ma, S. Formation of a Metalloporphyrin-Based Nanoreactor by Postsynthetic Metal–Ion Exchange of a Polyhedral-Cage Containing a Metal–Metalloporphyrin Framework. *Chem. – Eur. J.* **19**, 3297–3301 (2013).
8. Lions, M. *et al.* Insights into the mechanism of electrocatalysis of the oxygen reduction reaction by a porphyrinic metal organic framework. *Chem. Commun.* **53**, 6496–6499 (2017).
9. Liu, Y. *et al.* Chemical Adsorption Enhanced CO2 Capture and Photoreduction over a Copper Porphyrin Based Metal Organic Framework. *ACS Appl. Mater. Interfaces* **5**, 7654–7658 (2013).
10. Zhang, H. *et al.* Efficient Visible-Light-Driven Carbon Dioxide Reduction by a Single-Atom Implanted Metal–Organic Framework. *Angew. Chem. Int. Ed.* **55**, 14310–14314 (2016).
11. Kim, I. S. *et al.* The Synthesis Science of Targeted Vapor-Phase Metalâ€"Organic Framework Postmodification. *J. Am. Chem. Soc.* **142**, 242–250 (2019).
12. Tan, K. *et al.* Reactivity of Atomic Layer Deposition Precursors with OH/H2O-Containing Metal Organic Framework Materials. *Chem. Mater.* **31**, 2286–2295 (2019).
13. George, S. M. Atomic Layer Deposition: An Overview. *Chem. Rev.* **110**, 111–131 (2010).
14. Lee, S.-M. *et al.* Improved Mechanical Stability of Dried Collagen Membrane after Metal Infiltration. *ACS Appl. Mater. Interfaces* **2**, 2436–2441 (2010).
15. Gregorczyk, K. E. *et al.* Tuning the Tensile Strength of Cellulose through Vapor-Phase Metalation. *Chem. Mater.* **27**, 181–188 (2015).
16. Daubert, J. S. *et al.* Effect of Meso- and Micro-Porosity in Carbon Electrodes on Atomic Layer Deposition of Pseudocapacitive V2O5 for High Performance Supercapacitors. *Chem. Mater.* **27**, 6524–6534 (2015).
17. Bae, C., Kim, H., Kim, E., Park, H. G. & Shin, H. Atomic-Layer Deposition into 2- versus 3-Dimensionally Ordered Nanoporous Media: Pore Size or Connectivity? *Chem. Mater.* **30**, 4748–4754 (2018).
18. Diller, K. *et al.* In vacuo interfacial tetrapyrrole metallation. *Chem. Soc. Rev.* **45**, 1629–1656 (2016).
19. Zhang, L. B. *et al.* Chemical Infiltration during Atomic Layer Deposition: Metalation of Porphyrins as Model Substrates. *Angew. Chem.-Int. Ed.* **48**, 4982–4985 (2009).
20. Kim, S. J. *et al.* A Surface Chemical Reaction in Organic-Inorganic Materials Using a New Chemical Evaporation System. *Chem. Mater.* **27**, 4546–4551 (2015).
21. Avila, J. R. *et al.* Porphyrins as Templates for Site-Selective Atomic Layer Deposition: Vapor Metalation and in Situ Monitoring of Island Growth. *Acs Appl. Mater. Interfaces* **8**, 19853–19859 (2016).
22. Bétard, A., Zacher, D. & Fischer, R. A. Dense and homogeneous coatings of CPO-27-M type metal–organic frameworks on alumina substrates. *CrystEngComm* **12**, 3768–3772 (2010).
23. Zhao, Y. *et al.* Mesoscopic Constructs of Ordered and Oriented Metal–Organic Frameworks on Plasmonic Silver Nanocrystals. *J. Am. Chem. Soc.* **137**, 2199–2202 (2015).
24. Zhao, Z. *et al.* Atomic Layer Deposition Inducing Integration of Co, N Codoped Carbon Sphere on 3D Foam with Hierarchically Porous Structures for Flexible Hydrogen Producing Device. *Adv. Funct. Mater.* **29**, 1906365 (2019).
25. Zhao, Z. *et al.* Atomic layer deposition-induced integration of N-doped carbon particles on carbon foam for flexible supercapacitor. *J. Materiomics* **6**, 209–215 (2020).
26. Daubert, J. S. *et al.* Intrinsic limitations of atomic layer deposition for pseudocapacitive metal oxides in

porous electrochemical capacitor electrodes. *J. Mater. Chem. A* **5**, 13086–13097 (2017).
27. Gordon, R. G., Hausmann, D., Kim, E. & Shepard, J. A Kinetic Model for Step Coverage by Atomic Layer Deposition in Narrow Holes or Trenches. *Chem. Vap. Depos.* **9**, 73–78 (2003).
28. Kane, D., Davis, R. & Vanfleet, R. Penetration depth variation in atomic layer deposition on multiwalled carbon nanotube forests. *J. Vac. Sci. Technol. A* **37**, 030907 (2019).
29. Mondloch, J. E. *et al.* Vapor-Phase Metalation by Atomic Layer Deposition in a Metal–Organic Framework. *J. Am. Chem. Soc.* **135**, 10294–10297 (2013).
30. Lemaire, P. C., Lee, D. T., Zhao, J. & Parsons, G. N. Reversible Low-Temperature Metal Node Distortion during Atomic Layer Deposition of Al_2O_3 and TiO_2 on UiO-66-NH_2 Metal–Organic Framework Crystal Surfaces. *ACS Appl. Mater. Interfaces* **9**, 22042–22054 (2017).
31. Li, Z. *et al.* Sintering-Resistant Single-Site Nickel Catalyst Supported by Metal–Organic Framework. *J. Am. Chem. Soc.* **138**, 1977–1982 (2016).
32. Li, Z. *et al.* Size effect of the active sites in UiO-66-supported nickel catalysts synthesized via atomic layer deposition for ethylene hydrogenation. *Inorg. Chem. Front.* **4**, 820–824 (2019).
33. Klet, R. C. *et al.* Synthetic Access to Atomically Dispersed Metals in Metal–Organic Frameworks via a Combined Atomic-Layer-Deposition-in-MOF and Metal-Exchange Approach. *Chem. Mater.* **28**, 1213–1219 (2016).
34. Kim, I. S. *et al.* Targeted Single-Site MOF Node Modification: Trivalent Metal Loading via Atomic Layer Deposition. *Chem. Mater.* **27**, 4772–4778 (2015).
35. Rimoldi, M. *et al.* Atomic Layer Deposition in a Metal–Organic Framework: Synthesis, Characterization, and Performance of a Solid Acid. *Chem. Mater.* **29**, 1058–1068 (2017).
36. Gallington, L. C. *et al.* Regioselective Atomic Layer Deposition in Metal–Organic Frameworks Directed by Dispersion Interactions. *J. Am. Chem. Soc.* **138**, 13513–13516 (2016).
37. Fateeva, A. *et al.* A Water-Stable Porphyrin-Based Metal–Organic Framework Active for Visible-Light Photocatalysis. *Angew. Chem. Int. Ed.* **51**, 7440–7444 (2012).
38. Yang, F. *et al.* Tuning Internal Strain in Metal–Organic Frameworks via Vapor Phase Infiltration for CO2 Reduction. *Angew. Chem. Int. Ed.* **n/a**, (2020).
39. Hill, G. T. *et al.* Insight on the Sequential Vapor Infiltration Mechanisms of Trimethylaluminum with Poly(methyl methacrylate), Poly(vinylpyrrolidone), and Poly(acrylic acid). *J. Phys. Chem. C* **123**, 16146–16152 (2019).
40. Laubengayer, A. W. & Gilliam, W. F. The Alkyls of the Third Group Elements. I. Vapor Phase Studies of the Alkyls of Aluminum, Gallium and Indium1. *J. Am. Chem. Soc.* **63**, 477–479 (1941).
41. Hiraoka, Y. S. & Mashita, M. Ab initio study on the dimer structures of trimethylaluminum and dimethylaluminumhydride. *J. Cryst. Growth* **145**, 473–477 (1994).
42. GOUTERMAN, M. 1 - Optical Spectra and Electronic Structure of Porphyrins and Related Rings. in *The Porphyrins* (ed. DOLPHIN, D.) 1–165 (Academic Press, 1978). doi:10.1016/B978-0-12-220103-5.50008-8.
43. Yang, F. *et al.* Reversible and Irreversible Reactions of Trimethylaluminum with Common Organic Functional Groups as a Model for Molecular Layer Deposition and Vapor Phase Infiltration. *Adv. Mater. Interfaces* **4**, 10 (2017).
44. Haouas, M., Taulelle, F. & Martineau, C. Recent advances in application of 27Al NMR spectroscopy to materials science. *Prog. Nucl. Magn. Reson. Spectrosc.* **94–95**, 11–36 (2016).
45. Desimone, J. M., Stangle, M., Riffle, J. S. & McGrath, J. E. Aluminium-27 NMR studies of aluminiumporphyrins. *Makromol. Chem. Macromol. Symp.* **42–43**, 373–385 (1991).
46. Alben, J. O., Choi, S. S., Adler, A. D. & Caughey, W. S. INFRARED SPECTROSCOPY OF PORPHYRINS*. *Ann. N. Y. Acad. Sci.* **206**, 278–295 (1973).
47. Balan, E., Lazzeri, M., Morin, G. & Mauri, F. First-principles study of the OH-stretching modes of gibbsite. *Am. Mineral.* **91**, 115–119 (2006).

SYNOPSIS TOC

Implementation of Vapor Phase Infiltration technique to efficiently modify in-bulk a microporous porphyrin-based Metal Organic Framework.